Quantification of Neuroepithelial Bodies and Their Innervation in Fawn-Hooded and Wistar Rat Lungs

Jeroen Van Genechten, Inge Brouns, Geoff Burnstock, Jean-Pierre Timmermans, and Dirk Adriaensen

Department of Biomedical Sciences, Laboratory of Cell Biology and Histology, University of Antwerp—RUCA, Antwerp, Belgium; and Autonomic Neuroscience Institute, Royal Free and University College Medical School, London, United Kingdom

The Fawn-Hooded rat (FHR), a model for primary pulmonary hypertension, shows an unexplained hypersensitivity to airway hypoxia. Because pulmonary neuroepithelial bodies (NEBs) appear to express a functional oxygen-sensing mechanism and an extensive sensory innervation, possible changes in this system should be taken into consideration. In the present study a comparative analysis of NEBs and their selective innervation was performed in FHRs and Wistar control rats. In both rat strains, the number of NEBs was estimated to be around 3,500, $\sim$ 40% of which were innervated by vagal sensory calbindin D28k-immunoreactive (IR) nerve endings and $\sim$ 50% by spinal sensory calcitonin gene-related peptide (CGRP)-IR nerve terminals. The number of intrinsic pulmonary nitrergic neurons and the percentage of pulmonary NEBs revealing a nitrergic innervation were highly significantly lower in FHRs. In both FHRs and Wistar rats, a remarkable morphologic interaction was observed between the intrinsic nitrergic and the CGRP-IR sensory population contacting NEBs. Our findings suggest a possible link between the hypersensitivity to airway hypoxia observed in FHRs and a reduced intrinsic pulmonary nitrergic innervation, possibly via the interaction with pulmonary NEBs and their spinal sensory CGRP-IR innervation.

The Fawn-Hooded rat (FHR), a strain with a light yellowish brown hooded coat pattern, was originally studied because it displays a mild bleeding disorder (1) caused by a hereditary defect in platelet aggregation due to a malfunction of the serotonin (5-HT) uptake in platelets. Nowadays, the FHR is used among others to study mechanisms that determine susceptibility to primary pulmonary hypertension (PPH). This rat strain shows a congenital predisposition to PPH, which rapidly develops after exposure to even mild hypoxia (2, 3). Hypersensitivity to airway hypoxia was shown in FHRs in the perinatal period already (4). PPH is characterized by a progressive narrowing of the lumen of pulmonary vessels; the typical morphologic appearances of vascular remodeling include intimal fibrosis, medial muscularization, adventitial proliferation, and remarkable plexiform lesions (2, 5). As such, the FHR represents an interesting model to investigate factors that putatively determine a congenital susceptibility to pulmonary hypertension.

Because FHRs reveal a hypersensitivity to airway hypoxia (3), possible changes in the diffuse neuroendocrine system (DNES) of the lungs, the neuroendocrine cells of which have been shown to express a functional oxygen-sensing mechanism (6–9), have to be taken into consideration. Especially the extensively innervated aggregates of neuroendocrine cells, called neuroepithelial bodies (NEBs), which are diffusely spread in the epithelium at all levels of the intrapulmonary airways but are preferentially located at airway bifurcation points in rat lungs (10), might be involved. Neuroendocrine cells are able to synthesize and release ATP (11), monoamine, and peptide transmitters, resulting in autocrine, paracrine, neurocrine, or endocrine effects. NEBs morphologically resemble known chemoreceptors, such as taste buds and carotid bodies, and are, among other possible functions, thought to represent "chemosensors." Hypoxic conditions appear to depolarize NEB cells via a potassium channel–mediated mechanism (9, 12). NADPH oxidase was suggested to be the oxygen-sensing molecule (13, 14). Most likely, nerve fiber populations selectively innervating NEBs are involved in the reaction to hypoxia (15–17). Based on an ultrastructural analysis of rabbit NEBs, morphologically afferent-like as well as efferent-like nerve endings innervating NEBs were reported to be involved in the reaction of NEBs to acute hypoxia (18, 19).

Our own recent investigations disclosed that in rat lungs, NEBs receive an extensive and very complex innervation pattern (for review *see* Ref. 17). An intraepithelial vagal sensory innervation of NEBs, with origin in the nodose ganglion (20), appeared to be myelinated and was characterized by a calbindin D28k (CB) immunostaining (16) and the expression of purinergic $P2X_3$ receptors (11). A second sensory, capsaicin-sensitive, and calcitonin gene-related peptide (CGRP)/Substance P (SP)-immunoreactive (IR) innervation of NEBs, was shown to have a nonvagal origin (16, 20). Retrograde tracing experiments suggested a spinal origin for the latter sensory nerve fiber population (21). In addition, intrinsic pulmonary nitrergic neurons were seen to give rise to intraepithelial terminal arborizations that invariably colocalized with NEBs (15). Although Brouns and coworkers (22) reported NEBs that were selectively contacted by at least three different nerve fiber populations, clearly not all NEBs revealed identical combinations of

(*Received in original form March 21, 2003 and in revised form June 5, 2003*)

Address correspondence to: Dirk Adriaensen, Laboratory of Cell Biology and Histology, University of Antwerp—RUCA, Groenenborgerlaan 171, B-2020 Antwerp, Belgium. E-mail: dadria@ruca.ua.ac.be

Abbreviations: calbindin D28k, CB; calcitonin gene-related peptide, CGRP; diffuse neuroendocrine system, DNES; Fawn-Hooded rat, FHR; immunoreactive/immunoreactivity, IR; neuroepithelial bodies, NEBs; neuronal nitric oxide synthase, nNOS; nitric oxide, NO; overnight, ON; phosphate-buffered saline, PBS; protein gene product 9.5, PGP9.5; primary pulmonary hypertension, PPH; substance P, SP; tyrosine hydroxylase, TH; tyramide signal amplification, TSA; vesicular acetylcholine transporter, VAChT; vasoactive intestinal polypeptide, VIP.

Am. J. Respir. Cell Mol. Biol. Vol. 30, pp. 20–30, 2004
Originally Published in Press as DOI: 10.1165/rcmb.2003-0097OC on June 19, 2003
Internet address: www.atsjournals.org

nerve terminals. Furthermore, Adriaensen and coworkers (17) suggested that rat pulmonary NEBs are selectively contacted by additional nerve fiber populations, other than those described above. In an electron microscopic morphologic study of NEBs in FHR lungs, a very dense intraepithelial innervation of NEBs was reported and suggested to be considerably more extensive than in other species (23). Using NADPHd histochemistry in FHR lungs, we recently observed a decreased number of intrinsic pulmonary nitrergic neuronal cell bodies, or a reduced enzyme activity that hampers their visualization (24). It has been reported for carotid bodies that nitric oxide (NO) exerts an inhibitory influence on chemoreceptor activity (25). So far, however, it has not been clarified whether the lower number of intrinsic pulmonary nitrergic neurons in FHRs as compared with Wistar rats, also results in a lower percentage of NEBs that receive nitrergic nerve terminals (15). Neither are data available for the FHR on the many other nerve fiber populations described to selectively contact NEBs in Wistar rats (17).

It was the aim of the present study to unravel and quantify the complex selective innervation of NEBs in the FHR, and to compare the number and location of NEBs, and the different nerve fiber populations, between FHRs and Wistar control rats. The investigation was focused on young (10-d-old) FHR specimens that were known to have not yet developed PPH, to find differences that may explain the reported hypersensitivity of the strain to even very mild airway hypoxia. At least for now, it was decided not to perform the complex quantification in hypertensive specimens, because NEB literature data clearly revealed that PPH (26) appears to induce a strong proliferation of the pulmonary neuroendocrine system, which would complicate the sound interpretation of all other parameters in the context of hypersensitivity to airway hypoxia.

Materials and Methods

Animals

Ten-day-old (n = 11) and young adult (± 150 g; 5–6 wk old; n = 4) Wistar rats (Iffa Credo, Brussels, Belgium), and 10-d-old (n = 12) and young adult (± 150 g; 5–6 wk old; n = 2) FHRs (Elevage Janvier, Le Genet St. Isle, France) of both sexes were used in the present study. The rats were kept in acrylic cages in an acclimatized room (12/12 h light/dark cycle; 22 ± 3°C) and provided with water and food pellets *ad libitum*. National and international principles of laboratory animal care were followed and the experiments were approved by the local ethics committee of the University of Antwerp.

Tissue Processing

All animals were put to death using an overdose of sodium pentobarbital (Nembutal 200 mg/kg). After an intraperitoneal injection with heparin (500 U/kg; Rhône Poulenc Rorer 256S68F12; Brussels, Belgium) the rats were perfused via the right ventricle with a Krebs solution. Lungs were intratracheally instilled with fixative (4% phosphate-buffered paraformaldehyde). After 30 min, the lungs were dissected, degassed under vacuum, and immersion-fixed for an additional 2 h. Thereafter, the lungs were rinsed in phosphate-buffered saline (PBS; 0.01 M, pH 7.4). All tissue blocks were incubated overnight (ON) in 20% sucrose (in PBS; 4°C) and freeze-mounted in TissueTek (Sakura Finetek Europe, Zoetewoude, The Netherlands). Serial 25-μm-thick cryostat sections of the complete lungs were thaw-mounted on poly-L-lysine-coated microscope slides, air-dried, and stored at −80°C in a closed container until further use for immunocytochemistry.

Immunocytochemistry

All incubations were performed at room temperature in a humid incubation chamber. Primary and secondary antisera were diluted in PBS containing 10% normal serum of the species used to raise the secondary antibodies, 0.1% bovine serum albumin, 0.05% thimerosal, and 0.01% NaN_3 (PBS*). Characteristics and sources of all products used for immunocytochemistry are listed in Table 1. Before incubation with the primary antisera, cryostat sections were incubated for 30 min with PBS* containing 1% Triton-X-100. Washes with PBS were performed between each incubation. After a final wash, all sections were mounted in Citifluor (19470; Ted Pella, Redding, CA).

Conventional Immunocytochemical Labeling

Cryostat sections were incubated ON with one or a mixture of two primary antibodies raised in different species, and subsequently for 1 h with an appropriate mixture of secondary antisera. Sections labeled with a biotinylated secondary antiserum were additionally incubated for 1 h with a fluorochrome-conjugated streptavidin complex. The conventional single and double labelings used in the present study are described in detail in Table 2.

Double Staining Using Tyramide Signal Amplification

To obtain enhanced sensitivity and to allow the combination of two antisera raised in the same species, a biotinylated tyramide signal amplification (TSA) kit (NEL700; PerkinElmer Life Sciences, Boston, MA) was applied to visualize the first primary antibody. Before the immunocytochemical procedure, endogenous peroxidase was blocked by hydrogen peroxide (0.6% in 50% methanol/PBS, 20 min). For the first primary incubation, a rabbit polyclonal antibody against rat neuronal nitric oxide synthase (nNOS) (diluted 1:10,000, ON) was applied. Sections were then consecutively incubated with GAR-Fab-biot (diluted 1:2,000, 1 h) and ExtrAvidin-HRP (diluted 1:2,000 in PBS containing 0.05% thimerosal and 0.1% BSA, 1 h). Between subsequent steps, sections were washed in PBS containing 0.05% Tween 20. After rinsing, sections were incubated with biotinylated tyramide in "amplification solution" (diluted 1:100, 10 min) and visualization was performed using Str-Cy3 (diluted 1:6,000 in PBS, 10 min). To simultaneously demonstrate nNOS-IR nerve fibers and pulmonary NEBs, sections were subsequently subjected to conventional indirect immunocytochemical staining with rabbit polyclonal antibodies against CGRP (diluted 1:500, ON), CB (diluted 1:2,500, ON) or protein gene product 9.5 (PGP9.5; diluted 1:4,000, ON). These second primary antibodies were visualized using GAR-Fab-FITC (diluted 1:200, 1 h). TSA-enhanced immunostaining for SP and for the $P2X_3$ receptor was performed according to previously described methods (11, 16).

Control Experiments for Immunocytochemistry

Negative staining controls for all immunocytochemical procedures were performed by substitution of non-immune sera for the primary or secondary antisera. The general specificity of the primary antibodies for their respective antigens was tested by the providing companies, and the selectivity in rat lung sections in particular was extensively proven using positive and preabsorption controls as described in our previous publications (11, 15, 16). To check for cross-reactivity in any of the steps of the double staining proce-

TABLE 1
Products used for immunocytochemistry

Primary Antigen	Host	Mc/Pc	Source
Calbindin D-28k (CB)	Rabbit	Pc	Swant CB-38, Bellinzona, Switzerland
Calcitonin gene-related peptide (CGRP)	Rabbit	Pc	Affiniti CA1134, Exeter, UK
CGRP	Guinea Pig	Pc	EuroDiagnostica B-GP 470-1, Malmö, Sweden
Neuronal nitric oxide synthase (nNOS)	Mouse	Mc	Sigma N2280, Bornem, Belgium
nNOS	Rabbit	Pc	EuroDiagnostica B220–1
Protein gene product 9.5 (PGP9.5)	Rabbit	Pc	Biogenesis 7863–0504, Poole, UK
$P2X_3$ purinoreceptor ($P2X_3$)	Rabbit	Pc	Gift from Roche Bioscience, Palo Alto, CA
Substance P (SP)	Rabbit	Pc	Sigma S1542
Tyrosine hydroxylase (TH)	Mouse	Mc	Chemicon MAB5280, Temecula, CA
Vasoactive intestinal polypeptide (VIP)	Mouse	Mc	Biotrend 9535–0504, Cologne, Germany
Vesicular acetylcholine transporter (VAChT)	Rabbit	Pc	Phoenix H-V006, Belmont, CA
Secondary Antisera			**Source**
Biotinylated sheep anti-mouse immunoglobulin G (IgG) (ShAM-biot)			Amersham RPN 1001, Buckinghamshire, England
Biotinylated Fab fragments of goat anti-rabbit IgG (GAR-Fab-biot)			Rockland 811–1602,Gilbertsville, PA
Cy3-conjugated donkey anti-guinea pig IgG (DAGP-Cy3)			Jackson 706–165–148,West Grove, PA
Cy3-conjugated donkey anti-mouse IgG (DAM-Cy3)			Jackson 715–165–151
Cy3-conjugated goat anti-rabbit IgG (GAR-Cy3)			Jackson 111–165–144
FITC-conjugated donkey anti-guinea pig IgG (DAGP-FITC)			Jackson 706–095–148
FITC-conjugated Fab fragments of goat anti-rabbit IgG (GAR-Fab-FITC)			Jackson 111–097–003
Avidin and Streptavidin Complexes			
Cy3-conjugated streptavidin (Str-Cy3)			Jackson 016–160–084
FITC-conjugated streptavidin (Str-FITC)			Jackson 016–090–084
ExtrAvidin-horseradish peroxidase (ExtrAvidin-HRP)			Sigma E2886

dures, the results of single immunostaining for each substance were evaluated and compared with those observed after double labeling. In addition, omission of the primary antiserum of the second incubation was used as a control for double staining with two primary antisera raised in the same species.

Quantification and Statistical Analysis

The optical fractionator method (27) was used to estimate the total number of NEBs in rat lungs. In short, the number of NEBs in rat lungs was estimated by using the optical disector in combination with a systematically applied fractionator sampling scheme. The optical disector is an optical three-dimensional probe in which objects in a defined volume are counted directly. The disector consists of two parallel optical sections, a known distance apart, with uniform random probability of the object of interest. In the first section, particles are sampled according to the two-dimensional unbiased counting and sampling rule, only counting particles present in the sampling frame and not in the second section (28). This method provides an estimate of the particle number, unbiased by size, shape, or orientation. The disector principle guarantees that each particle is counted only once. Consequently, the counted number is associated with a defined volume (the disector), the space equal to the counted area multiplied by the distance between the pairs of sections. In the fractionator method, a structure is systematically subdivided into smaller fractions. The number of particles is estimated in the well-defined fraction and related back to the volume of the whole structure.

TABLE 2
Conventional single and double staining procedures

First Primary Antisera	Dilution	Secondary and Tertiary Reagents	Dilution	Second Primary Antisera	Dilution	Secondary and Tertiary Reagents	Dilution
CGRP	1/2,000	DAGP-FITC	1/100				
CGRP	1/2,000	DAGP-Cy3	1/200	CB	1/2,000	GAR-Fab-FITC	1/200
VAChT	1/4,000	GAR-Cy3	1/2,000	nNOS	1/1,000	ShAM-biot	1/200
						Str-FITC	1/1,000
TH	1/20	DAM-Cy3	1/200	PGP9.5	1/4,000	GAR-Fab-FITC	1/200
VAChT	1/4,000	GAR-Cy3	1/2,000	CGRP	1/2,000	DAGP-FITC	1/100
VIP	1/2,000	ShAM-biot	1/200	CGRP	1/2,000	DAGP-FITC	1/100
		Str-Cy3	1/4,000				

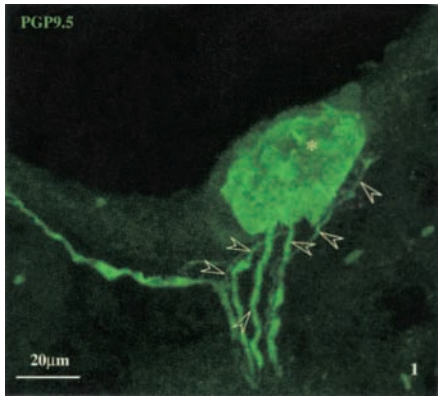

Figure 1. The PGP9.5-IR neuroepithelial body (NEB; *asterisk*), located at an airway bifurcation, is contacted by profuse nerve terminals (*open arrowheads*). Maximum intensity projection of 25 confocal optical sections (1.0-μm interval).

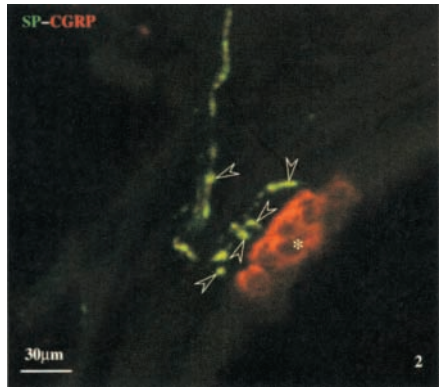

Figure 2. TSA-enhanced immunocytochemical staining for SP (*green FITC fluorescence*) and sequential conventional staining for CGRP (*red Cy3 fluorescence*). The CGRP-IR NEB (*asterisk*) receives a complex of CGRP/SP-IR spinal sensory nerve terminals (*open arrowheads*; *yellow color*), which appear to contact the NEB basally. Maximum intensity projection of nine confocal optical sections (1.0-μm interval).

The total number of NEBs was estimated by two pairs of optical confocal sections (LSM 510; Zeiss, Zaventem, Belgium), separated by 20 μm within a pair, and by 375 μm between the pairs. Solitary neuroendocrine cells were not taken into account in the present study. Because of the highly diffuse distribution of NEBs, whole sections were counted. The disector was, therefore, defined by the surface area of the transverse lung sections and the height of the optical disector. When applying the fractionator method, the surface area of the lung was assumed to be constant between the two pairs of optical sections, leaving the height as the only variable. Consequently, the total number of NEBs in the lungs per animal was estimated by multiplying the number of NEBs counted per height of the disectors by the total height of the lungs. Whether data obtained by different markers could be grouped was analyzed by one-way ANOVA. The average total number of NEBs per animal, presented as means ± SEM, was compared between age-matched FHRs and Wistar rats and between differently aged rats of the same strain, and analyzed by the Student's *t* test.

For comparative quantitative analysis of the number of neuronal cell bodies and nerve fiber populations that selectively contact the NEBs, every fifth section of the series of complete serially sectioned lungs of an animal was examined. Again, whole sections had to be screened because the density of the investigated structures appeared very low. For each animal, the percentage of NEBs contacted by a specific nerve fiber population was calculated using the ratio of NEBs receiving the particular nerve terminals to all counted NEBs. Whether data obtained by different immunocytochemical procedures could be grouped was analyzed by ANOVA. The ratio of the numbers of nitrergic neuronal cell bodies to the numbers of NEBs innervated by nNOS-IR nerve terminals was also evaluated.

The distribution of the NEBs and of the nerve fiber populations that selectively contact the NEBs along the airway levels, was analyzed by calculating the proportion of the quantified structures at different predefined levels, i.e., bronchi, bronchioles, terminal and respiratory bronchioles, and alveolar areas, in relation to the total number of quantified structures counted per animal.

All average numbers, ratios, or percentages of quantified structures in different animals, presented as means ± SEM, were compared between age-matched FHRs and Wistar rats and between differently aged rats of the same strain, and analyzed by the Student's *t* test. In all analyses, a probability of $P < 0.05$ was set as the level of significance.

Microscopic Analysis

An epifluorescence microscope (Zeiss Axiophot) equipped with filters for the visualization of FITC (Zeiss 17; BP 485–20/ FT 510/ BP 515–565) and Cy3 (Zeiss 14; LP 510-KP 560/ FT 580/ LP 590) was used to evaluate the results and to perform the quantitative analysis. For detailed imaging and optical sectioning, a confocal laser scanning microscope (Zeiss LSM 510) equipped with image reconstruction facilities (Imaris 2.7 software; Bitplane AG, Zürich, Switzerland; Silicon Graphics Indigo 2 workstation) was used. A helium-neon laser (543 nm) and an argon laser (488 nm) were used for the excitation of Cy3 and FITC, respectively.

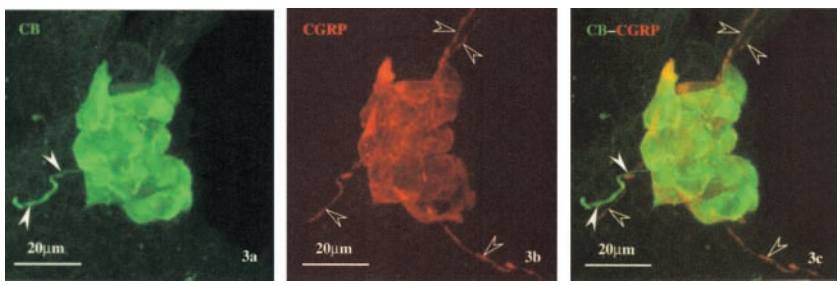

Figure 3. Conventional immunocytochemical double staining for CB (*green FITC fluorescence*) and CGRP (*red Cy3 fluorescence*) using antibodies raised in different species. (*a*) A bronchiolar CB-IR NEB is innervated by a thick CB-IR nerve fiber (*arrowheads*). (*b*) The same NEB also shows CGRP IR and is innervated by varicose CGRP-IR nerve terminals (*open arrowheads*). (*c*) Combination of both channels revealing a double-labeled NEB contacted by clearly separate populations of CB- and CGRP-IR nerve fibers. Maximum intensity projections of 41 confocal optical sections (0.8-μm interval).

Results

Unless otherwise indicated, all data were obtained from 10-d-old rats.

Control Experiments

Substitution of nonimmune sera for primary and secondary antisera resulted in negative staining controls in all immunocytochemical procedures performed. In double immunolabelings using TSA-enhanced and subsequent conventional staining, omission of the primary antiserum of the second incubation abolished all immunostaining for the second antigen. None of the investigated parameters yielded significant differences between different animals or between male and female animals from the same strain. Therefore, they were regarded as one group in all cases.

Pulmonary Neuroepithelial Bodies in 10-d-old Rats

In both rat strains, NEBs were easily detected by each of the pulmonary neuroendocrine cell markers used: PGP9.5, CGRP, and CB (Figures 1–7). The data for all markers were grouped because no significant differences in the total number of NEBs were found between the labels. Based on the optical fractionator method, the number of NEBs in 10-d-old rat lungs was estimated to be around 3,500 (Table 3) and did not differ significantly between Wistar rats and FHRs. In both rat strains, NEBs were observed in the epithelium at all levels of intrapulmonary airways: from bronchi to alveoli (Table 4). Proportionally, most NEBs were found in bronchioles, and terminal and respiratory bronchioles. Again, no significant differences in the distribution of NEBs along the airways were found between FHRs and Wistar rats.

The Vagal and Spinal Sensory Innervation of NEBs

The vagal, CB/$P2X_3$-IR, nerve population that makes intraepithelial contact with NEBs (Figures 4–5) innervates $\sim$ 40% of the NEBs in both FHRs and Wistar rats (Table 5). Although the percentage of NEBs that are basally innervated by spinal, CGRP/SP-IR, nerve terminals (Figure 2) is similar in both rat strains ($\sim$ 50%), a small but significant difference was observed (Table 5). NEBs innervated by vagal and/or spinal sensory nerve fibers were observed all along the airways (Tables 6 and 7). A conventional immunocytochemical double staining using antibodies against CB and CGRP, raised in rabbit and guinea pig, respectively, was used to determine the percentage of NEBs receiving both vagal and spinal sensory nerve terminals (Table 5; Figure 3). About 30% of the NEBs appeared to be innervated by both afferent nerve fiber populations, implying that, in both rat strains, $\sim$ 60% of the NEBs were contacted by at least one of these sensory populations.

Intrinsic Pulmonary Nitrergic Neurons and Innervation of NEBs in 10-d-old Rats

The intrinsic pulmonary nitrergic innervation was analyzed by nNOS immunocytochemistry. Simultaneously, NEBs were visualized as mentioned above. Nitrergic neuronal cell bodies in the lamina propria of the airways (Figures 8a and 8b) could be unambiguously identified using a conventional immunocytochemical staining. Intraepithelial nitrergic nerve terminals, which invariably colocalized with NEBs (Figures 6–7), could only be seen after TSA amplification. The data from different nNOS-immunocytochemical double stainings were pooled because no significant differences were found.

The percentage of NEBs that received a nitrergic innervation (Table 8) was significantly lower in the FHR ($\sim$ 2.8%) than in the Wistar rat ($\sim$ 10.6%). In both rat strains, NEBs receiving nNOS-IR nerve fibers were observed at all airway levels, from large conductive airways to gas-exchange areas (Table 9). Similarly, a significantly reduced number (P = 0.0001) of intrinsic pulmonary nitrergic neurons was detected in FHRs as compared with Wistar rats. In Wistar rat lungs, a mean number per animal of 182 cell bodies was counted in the selected sections, whereas in identically sampled FHR lungs, only 41 were seen. Remarkably, intrinsic pulmonary nitrergic cell bodies, appearing solitary or grouped in small ganglia, were always surrounded by baskets of varicose CGRP-IR nerve fibers (Figure 8a). No obvious morphologic interaction was observed between CB-IR nerve fibers and the intrinsic nitrergic neurons.

Despite a significantly lower number of intrinsic nitrergic neurons and nitrergic innervated NEBs in FHRs, the ratio of nitrergic cell bodies to nitrergic innervated NEBs was $\sim$ 3:2, and not significantly different between FHRs and Wistar rats (Table 8).

In both FHRs and Wistar rats, NEBs showed a considerable overlap between nitrergic and sensory innervation (Table 10). Remarkably, all NEBs revealing nitrergic nerve terminals were also contacted by CGRP-IR spinal sensory fibers (Figure 7).

Part of the nitrergic innervated NEBs were seen to receive additional CB-IR vagal sensory nerve terminals (Figure 6). A significant difference, however, was observed in the percentage of NEBs that were contacted by both nitrergic and vagal sensory fibers between Wistar rats ($\sim$ 57%) and FHRs ($\sim$ 85%).

Quantification of Pulmonary NEBs and their Nitrergic Innervation in Young Adult Rats

No significant differences were observed in the total number of NEBs, characterized by their CGRP IR, when comparing 10-d-old and young adult rats of the same strain, although NEBs appeared to be slightly more numerous in the young adults (compare Tables 3 and 11). Similar to the 10-d-old rats, no significant difference in the total number of NEBs was found between young adult FHRs and Wistar rats (Table 11).

Combination of nNOS and CGRP immunocytochemistry revealed also in young adult rats a significantly reduced number of intrinsic pulmonary nitrergic neuronal cell bodies. In Wistar rat lungs, a mean number per animal of 153 nitrergic neurons was counted in the selected sections, whereas in identically sampled FHR lungs, only 22 were seen. Similarly, the percentage of NEBs that received a nitrergic innervation in FHR lungs was significantly lower than in Wistar rat lungs (Table 11). Also in the young adult rats, all nitrergic innervated NEBs appeared to be contacted by CGRP-IR spinal sensory nerve fibers.

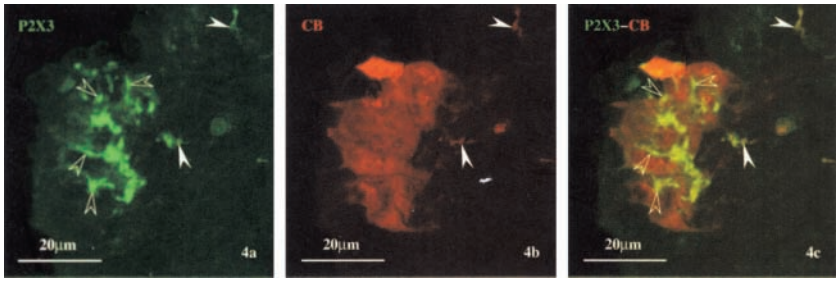

Figure 4. Immunocytochemical double staining for $P2X_3$ receptors (*green FITC fluorescence*; TSA-enhanced) and CB (*red Cy3 fluorescence*). (*a*) *Green channel* showing a $P2X_3$-IR nerve fiber (*arrowheads*) that gives rise to an intraepithelial terminal arborization (*open arrowheads*). (*b*) *Red channel* showing a bronchiolar CB-IR NEB (*asterisk*) contacted by a CB-IR nerve fiber (*arrowheads*). (*c*) Combined image revealing that the CB-IR NEB receives nerve terminals that co-localize CB and $P2X_3$ IR and arborize between the neuroendocrine cells. Maximum intensity projections of 39 confocal optical sections (0.4-μm interval).

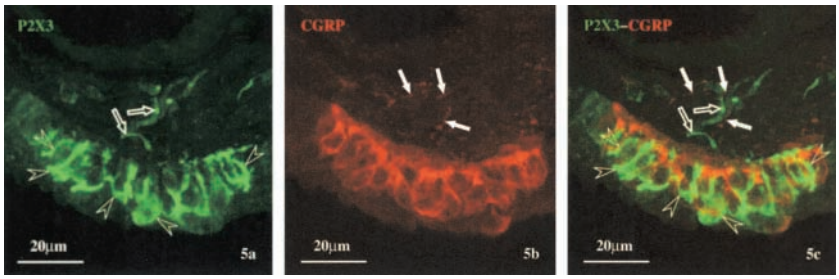

Figure 5. Immunocytochemical double staining for $P2X_3$ receptors (*green FITC fluorescence*; TSA-enhanced) and CGRP (*red Cy3 fluorescence*). (*a*) *Green channel* showing intraepithelial $P2X_3$-IR nerve terminals (*open arrowheads*), which originate from subepithelial nerve fibers (*open arrows*). (*b*) *Red channel* showing thin varicose CGRP-IR nerve fibers (*arrows*) that contact a CGRP-IR bronchiolar NEB. (*c*) Combined image revealing that the $P2X_3$ purinoreceptor-IR intraepithelial nerve fibers arborize between the CGRP-IR NEB cells. The CGRP-IR nerve terminals are clearly different from those expressing $P2X_3$ receptors. Maximum intensity projections of 33 confocal optical sections (0.4-μm interval).

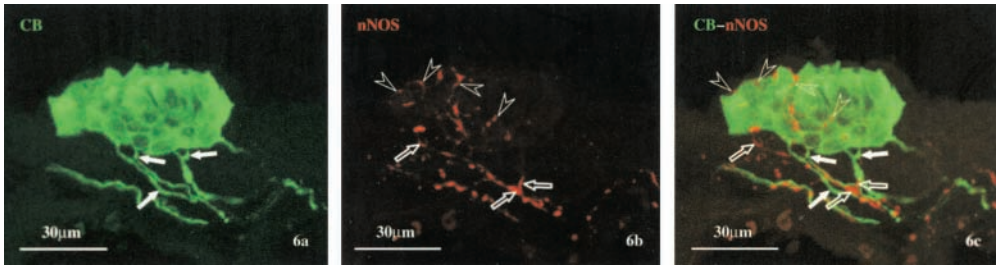

Figure 6. TSA-enhanced immunostaining for nNOS (*red Cy3 fluorescence*) combined with conventional immunocytochemistry to detect CB (*green FITC fluorescence*). (*a*) *Green channel* revealing profuse CB-expressing nerve endings (*arrows*) that enter a CB-IR NEB. (*b*) *Red channel* showing nNOS-IR nerve fibers (*open arrows*) that give rise to intraepithelial nerve terminals (*open arrowheads*). (*c*) Combination of both channels reveals that the nitrergic terminals are co-localized with the NEB and are clearly different from the CB-IR nerve fibers. Maximum intensity projections of 17 confocal optical sections (1.0-μm interval).

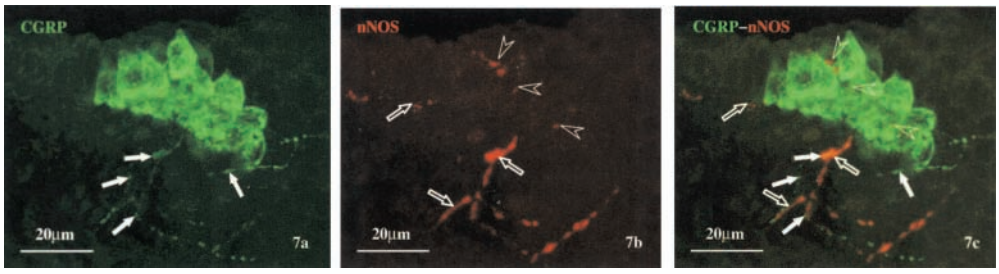

Figure 7. Immunocytochemical double staining for nNOS (*red Cy3 fluorescence*) and CGRP (*green FITC fluorescence*). (*a*) *Green channel* showing a bronchiolar CGRP-IR NEB receiving CGRP-IR nerve endings (*arrows*). (*b*) *Red channel* showing intraepithelial nNOS-IR nerve terminals (*open arrowheads*) protruding between the pulmonary neuroendocrine cells and originating from subepithelial nitrergic nerve fibers (*open arrows*). (*c*) Combined image revealing that the nitrergic and CGRP-IR terminals belong to different nerve fiber populations, although some of the CGRP-IR nerve terminals are in very close proximity to the nNOS-IR nerve fibers. Note that the intraepithelial nitrergic nerve endings run between the neuroendocrine cells and appear to reach the luminal surface of the NEB. Maximum intensity projections of 28 confocal optical sections (0.5-μm interval).

TABLE 3
Mean number of pulmonary NEBs per rat

	n	Number of NEBs per Animal Based on the Optical Fractionator Method
Wistar rat	9	3,934 ± 294
FHR	10	3,162 ± 230

Data are expressed as mean ± SEM; *n*, number of animals.

TABLE 4
Proportional distribution of NEBs along the airways per rat

	n	Mean Percentage of NEBs in Bronchi	Mean Percentage of NEBs in Bronchioles	Mean Percentage of NEBs in Terminal Bronchioles and Respiratory Areas
Wistar rat	9	5.9 ± 0.8%	37.6 ± 2.0%	56.5 ± 2.5%
FHR	10	4.7 ± 1.0%	33.6 ± 1.0%	61.7 ± 1.2%

Data are expressed as mean ± SEM; *n*, number of animals.

Other Nerve Fiber Populations Innervating Pulmonary NEBs in the FHR

To further illustrate the complexity of the selective innervation of pulmonary NEBs in FHRs, we performed several additional immunocytochemical stainings in 10-d-old rats. Cholinergic, vesicular acetylcholine transporter (VAChT)-IR and nNOS-negative, neuronal cell bodies were abundant in large parasympathetic ganglia in the hilar region of the lungs and surrounding extrapulmonary airways. More rare cholinergic but non-nitrergic cell bodies were also seen in small ganglia in the lamina propria of mainly large intrapulmonary airways (Figures 8c and 9a). An extensive network of VAChT-IR nerve fibers, most likely originating in intrinsic neurons, was seen in airway smooth muscle bundles (Figures 8b and 9a). Some VAChT-IR nerve terminals, with unknown origin, appeared to show basal contacts with NEBs, and sometimes were even seen in the epithelium between the neuroendocrine cells (Figures 9b and 9c). Furthermore, the neuroendocrine cells composing NEBs displayed a mostly weak VAChT IR (Figure 9b).

A considerable number of NEBs were seen to be innervated by an extensive intraepithelial plexus of vasoactive intestinal polypeptide (VIP)-IR nerve terminals (Figure 10).

Adrenergic, tyrosine hydroxylase (TH)-IR nerve fibers were found in vascular smooth muscle and in parasympathetic ganglia. Also, TH-IR nerve fibers appeared to contact some of the NEBs (Figure 11).

Discussion

The present study was designed to document the DNES and its complex innervation pattern in FHR lungs, and to compare it with our current knowledge of the system in Wistar rats (11, 15–17).

No significant differences were found in the total number of pulmonary NEBs or in their distribution along the airways between FHRs and Wistar rats. Both in FHR and Wistar rat lungs (PD 10), the total number of NEBs was estimated to be between 3,000 and 4,000, with ~40% receiving vagal CB/P2X$_3$-IR nerve terminals, and ~ 50% spinal CGRP/SP-IR nerve terminals. About 30% of NEBs were innervated by both sensory nerve fiber populations, and ~ 60% by at least one of the populations. Considering the dual sensory innervation of NEBs in both FHRs and Wistar rats, the sensory nature of pulmonary NEBs seems beyond dispute, suggesting that they represent an extensive population of intraepithelial airway receptors.

The present study provides evidence that NEBs in FHR lungs may, in addition to an intraepithelial vagal sensory innervation, a basal spinal sensory innervation, and an intraepithelial nitrergic innervation, receive several other nerve fiber populations that provide additional nervous connections to NEBs. VAChT was found to be a selective marker for cholinergic neurons in the peripheral nervous system (29). At the moment, no conclusive data are available about the nature and origin of the cholinergic nerve terminals contacting NEBs. Both in FHRs and Wistar rats, a considerable number of NEBs appear to be contacted by profuse, beaded VIP-IR nerve terminals. Although a weak VIP IR was seen to be localized in the intrinsic nitrergic neurons that give rise to nitrergic terminals in NEBs in Wistar rats (17), we believe that an additional population of VIP-IR nerve endings with an as yet unidentified origin may be involved in the selective innervation of NEBs. Preliminary data further revealed that TH-IR nerve terminals selectively contact some pulmonary NEBs in FHRs and Wistar rats. Although not experimentally proven so far, the latter TH-IR nerve fibers likely have their origin in sympathetic ganglia. No obvious differences were observed in the VAChT-, VIP-, or TH-IR nerve fiber populations contacting NEBs between FHRs and Wistar rats. Although neither the cholinergic, nor the adrenergic or VIP-ergic nerve populations are fully characterized at the moment, it is important to realize that NEBs are extremely complex airway receptors in both FHRs and Wistar rats.

An electron microscopic study of FHR NEBs reported exceptionally densely innervated NEBs that harbor "clusters" of nerve fibers located intraepithelially between the neuroendocrine cells (23). We were, however, unable to confirm the impression that NEBs of the FHR model receive a more dense innervation than, e.g., NEBs in Wistar rat lungs. In contrast, the present comparison between FHRs and Wistar control rats revealed highly significantly lower numbers of NEBs receiving intraepithelial nNOS-IR nerve terminals, whereas for all other nerve fiber populations a similar percentage of innervated NEBs was observed in Wistar rats and FHRs. In the same electron microscopic study, efferent- and afferent-like terminals that colocalized with NEBs, were quantified. These nerve terminals were interpreted as belonging to a single population of sensory nerve fibers, presenting intraepithelial efferent-like collaterals, because vagotomy experiments resulted in a clearly reduced number of nerve terminals in NEBs, whereas the ratio of afferent- to efferent-like terminals appeared unchanged in the selected NEBs. It was further concluded that unlike in rabbits, a separate motor innervation of NEBs was probably nonexisting in rat lungs. Our data, obtained through neuronal tracing, chemical and mechanical denervations, and (immuno)cytochemistry, in combination with confocal microscopy, pointed out that in pulmonary NEBs

TABLE 5
Mean percentage of vagal or spinal sensory innervated NEBs

	Percentage of Vagal Sensory Innervated NEBs	Percentage of Spinal Sensory Innervated NEBs	Percentage of NEBs Innervated by Both Sensory Populations
Wistar rat	36.43 ± 2.09% (6,493/5)	56.10 ± 1.74% (4,392/4)	29.30 ± 0.67% (2,276/2)
FHR	36.93 ± 2.26% (5,642/5)	48.03 ± 2.42%* (4,480/5)	29.75 ± 4.37% (2,155/2)

Data are expressed as mean ± SEM; numbers in parentheses refer to number of NEBs counted/number of animals studied.
* $P = 0.037$.

of both FHRs and Wistar rats, vagal nodose sensory, intrinsic nitrergic, VIP-IR, and cholinergic motor terminals all appeared to penetrate between the neuroendocrine cells of NEBs, thus providing clear evidence for the existence of more than just one intraepithelial nerve fiber population. Therefore, the many nerve endings that were reported intact in the ipsilateral lungs after unilateral infranodosal vagotomy (23) do not necessarily reflect a crossing-over of intact contralateral vagal afferent fibers.

In addition to yielding an optimal nNOS immunodetection, TSA allowed us to combine antibodies originating in the same species. We are confident that in the present study, double labeling with two antisera raised in the same species, using TSA, was specific because omission of the second primary antisera invariably led to negative results for the second label, and no obvious differences could be observed when the antisera were evaluated after single immunostaining. In addition, substitution of nonimmune sera for primary or secondary antisera expectedly resulted in negative staining for all immunocytochemical procedures.

The large-scaled quantifications in the present study were performed on 10-d-old rats because at this age, the number of NEBs and their nitrergic innervation appeared to be similar to that in the lungs of young adult rats, whereas their density is considerably higher due to the much smaller lung volume. Moreover, our more limited control quantification (number of intrapulmonary nitrergic neurons and NEBs that receive nitrergic nerve terminals) in young adult Wistar rats and FHRs, of a similar age as used by other investigators to demonstrate hypoxia-induced pulmonary hypertension in FHRs (3), revealed no significant differences with 10-d-old specimens.

With respect to a possible explanation for the hypersensitivity to airway hypoxia observed in FHRs, the most interesting finding in the present study was a highly significantly smaller percentage of NEBs that receive intraepithelial nitrergic nerve terminals in 10-d-old as well as young adult FHRs as compared with age-matched Wistar control rats, and the additional confirmation of a lower number of intrinsic pulmonary nitrergic neurons in FHR lungs by nNOS immunocytochemistry. The observation of equally decreased numbers of intrinsic pulmonary nNOS-IR neurons and nitrergic innervated NEBs in FHRs strengthens the suggestion that the arborizing intraepithelial nitrergic nerve terminals in NEBs originate from intrinsic nitrergic neurons. The latter population of intrapulmonary neurons appears to be noncholinergic and therefore does not easily fit into the classical "parasympathetic concept." Several other investigators, however, have reported before that the airways of different species reveal rather complexly organized, often multilayered plexuses, which harbor interconnecting populations of cholinergic and nonadrenergic noncholinergic neurons (30–32).

In the carotid body, the significance of NO, at least partially derived from nNOS in the nerve plexuses innervating the chemoreceptor tissue, has been reviewed (33). Potent inhibitors of NOS appear to increase the sensory discharge of glomus cells, whereas NO donors reduce carotid body activity (34), suggesting that NO, continuously produced under basal conditions, exerts an inhibitory influence on the sensory discharge of glomus cells. Also, a marked argumentation of hypoxic responses was reported in nNOS knockout mice (35). Because of the accumulating evidence (*see* introduction) that pulmonary NEBs function as hypoxia-sensitive airway chemoreceptors, the nitrergic system demonstrated in NEBs may have a similar functional significance as suggested for carotid body cells. NO released from the terminals of intrinsic pulmonary nitrergic neurons may inhibit the sensory discharge of NEBs in response to, e.g., local hypoxia, and consequently a strong reduction of the nitrergic innervation in FHRs might explain the reported hypersensitivity to airway hypoxia.

TABLE 6
Proportional distribution of vagal (CB-IR) sensory innervated NEBs along the airways

	n	Mean Percentage of Vagal Sensory Innervated NEBs in Bronchi	Mean Percentage of Vagal Sensory Innervated NEBs in Bronchioles	Mean Percentage of Vagal Sensory Innervated NEBs in Terminal Bronchioles and Respiratory Areas
Wistar rat	5	10.3 ± 2.2%	38.8 ± 1.2%	50.8 ± 2.5%
FHR	5	8.5 ± 1.2%	42.6 ± 5.4%	48.7 ± 6.1%

Data are expressed as mean ± SEM; *n*, number of animals.

TABLE 7
Proportional distribution of spinal (CGRP-IR) sensory innervated NEBs along the airways

	n	Mean Percentage of Spinal Sensory Innervated NEBs in Bronchi	Mean percentage of Spinal Sensory Innervated NEBs in Bronchioles	Mean Percentage of Spinal Sensory Innervated NEBs in Terminal Bronchioles and Respiratory Areas
Wistar rat	4	9.0 ± 1.6%	45.4 ± 1.8%	45.6 ± 0.5%
FHR	5	9.3 ± 1.1%	44.1 ± 2.0%	46.5 ± 2.5%

Data are expressed as mean ± SEM; n: number of animals.

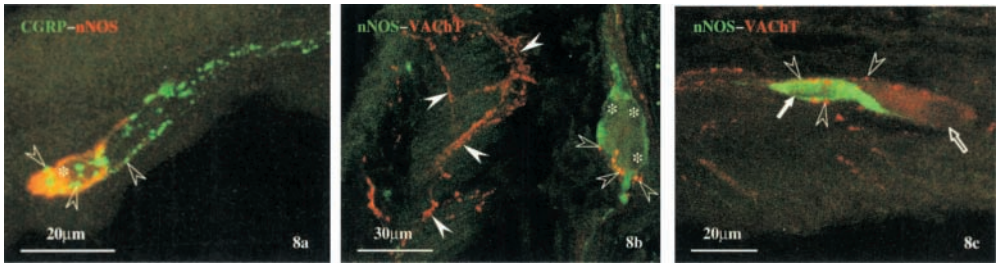

Figure 8. Details of intrinsic pulmonary nitrergic and cholinergic neurons in FHR lungs. (*a*) A solitary nitrergic (*red Cy3 fluorescence*) neuronal cell body (*asterisk*) surrounded by a basket of varicose CGRP-IR (*green FITC fluorescence*) nerve fibers (*open arrowheads*). Note the close association of nitrergic neuronal processes and CGRP-IR fibers. Maximum intensity projection of 14 confocal optical sections (0.7-μm interval). (*b*) A small ganglion showing three nitrergic neurons (*asterisks*; *green FITC fluorescence*) surrounded by baskets of cholinergic VAChT-IR (*red Cy3 fluorescence*) nerve fibers (*open arrowheads*). Note the extensive cholinergic innervation (*arrowheads*) of airway smooth muscle. Maximum intensity projection of seven confocal optical sections (1.0-μm interval). (*c*) A small ganglion composed of a nNOS-IR (*arrow*; *green FITC fluorescence*) and a VAChT-IR (*open arrow*; *red Cy3 fluorescence*) neuron. Cholinergic nerve fibers (*open arrowheads*) surround both neurons. Maximum intensity projection of 13 confocal optical sections (0.95-μm interval).

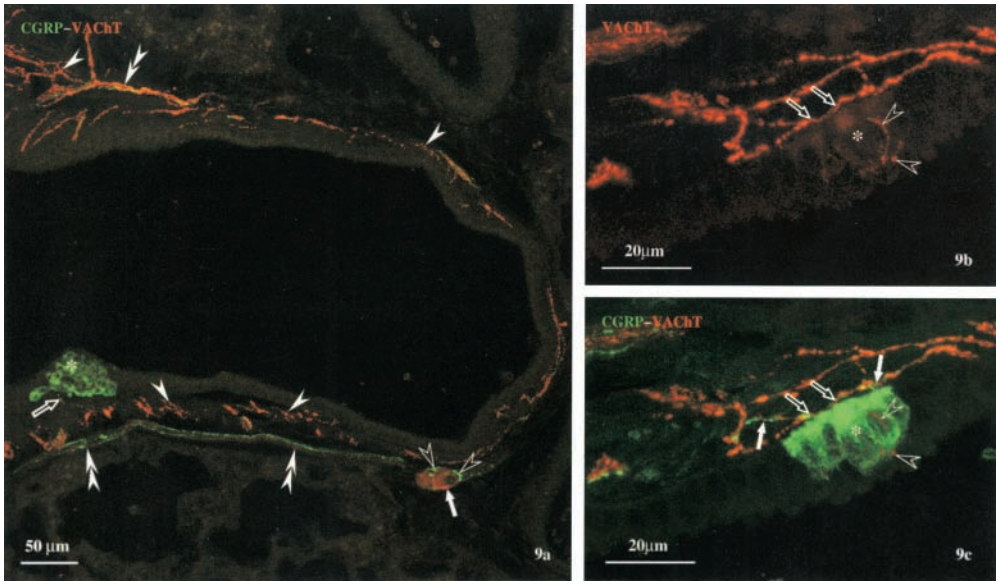

Figure 9. Conventional immunocytochemical double staining for VAChT (*red Cy3 fluorescence*) and CGRP (*green FITC fluorescence*). (*a*) Combined overview image revealing a CGRP-IR NEB (*asterisk*) protruding in the bronchiolar lumen, receiving a VAChT-IR nerve fiber (*open arrow*). A VAChT-IR ganglion (*arrow*), the neurons of which are closely surrounded by CGRP-IR nerve fibers (*open arrowheads*), is seen. The airway smooth muscle receives an extensive VAChT-IR innervation (*arrowheads*). Nerve bundles (*double arrowheads*) containing VAChT-IR and CGRP-IR nerve fibers are seen in the airway wall. Maximum intensity projection of 20 confocal optical sections (0.8-μm interval). (*b*, *c*) Details of an NEB (*asterisks*). (*b*) *Red channel* showing very weak VAChT IR (*red Cy3 fluorescence*) in the NEB that is basally contacted by a cholinergic nerve fiber (*open arrows*). Also note cholinergic nerve endings (*open arrowheads*) between the NEB cells. (*c*) CGRP IR confirms the location of the NEB and further reveals CGRP-IR nerve terminals (*arrows*) innervating the NEBs. Maximum intensity projections of 38 confocal optical sections (0.4-μm interval).

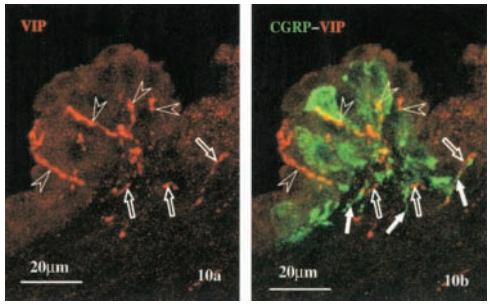

Figure 10. Conventional immunocytochemical double staining for VIP (*red Cy3 fluorescence*) and CGRP (*green FITC fluorescence*). (*a*) *Red channel* showing a subepithelial VIP-ergic nerve fiber (*open arrows*) that branches and gives rise to an intraepithelial VIP-IR arborization (*open arrowheads*). (*b*) Combined *red* and *green channels* revealing the presence of a CGRP-IR NEB. Besides the VIP-ergic innervation, the NEB also receives CGRP-IR nerve terminals (*arrows*). Maximum intensity projections of 19 confocal optical sections (0.7-μm interval).

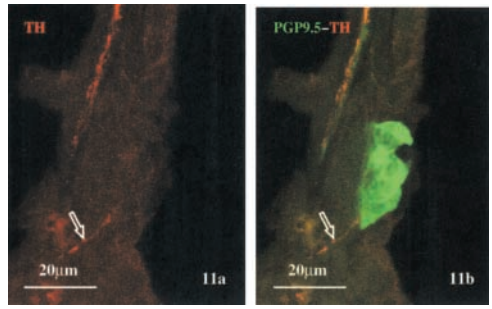

Figure 11. Conventional immunocytochemical double staining for TH (*red Cy3 fluorescence*) and PGP9.5 (*green FITC fluorescence*). (*a*) *Red channel.* A TH-IR nerve fiber (*open arrow*) approaches the bronchiolar epithelium. (*b*) Combined image. Using the neuronal marker PGP9.5, the adrenergic nerve fiber appears to make contact to an NEB. Maximum intensity projections of 19 confocal optical sections (0.6-μm interval).

TABLE 8
Mean percentage of nitrergic innervated NEBs

	Percentage of Nitrergic Innervated NEBs	Ratio of Nitrergic Cell Bodies to Nitrergic Innervated NEBs
Wistar rat	10.61 ± 1.12% (8,611/7)	1.51 ± 0.21
FHR	2.75 ± 0.36%* (8,044/7)	1.75 ± 0.35

Data are expressed as mean ± SEM; numbers in parentheses refer to number of NEBs counted/number of animals studied.
* $P = 0.0002$.

When the nitrergic innervation of NEBs was visualized in combination with sensory nerve terminals, both in Wistar rats and in FHRs, all nitrergic innervated NEBs also appeared to receive CGRP-IR spinal sensory nerve fibers, although only 50% of the total number of NEBs showed such a CGRP-IR innervation. Moreover, in FHR lungs, a similar reduction in the percentage of nitrergic and CGRP-IR innervated NEBs was noticed. In this context, it was also shown that nitrergic cell bodies located solitarily or in small ganglia in the lamina propria of intrapulmonary airways were always surrounded by baskets of varicose CGRP-IR nerve fibers. The latter terminals were suggested to be collaterals of the CGRP-IR nerve fibers that selectively contact NEBs (15). *In vitro* experiments have shown that the neuropeptide CGRP is a potent vasodilator of precontracted pulmonary arteries (36) and CGRP has been ascribed an important role in pulmonary pressure homeostasis during hypoxia (37). Tjen-A-Looi and coworkers (38) suggested that a capsaicin-sensitive CGRP-IR sensory nerve population is required for endogenous CGRP (from neuroendocrine cells) to modulate pulmonary vascular tone in hypoxia-induced pulmonary hypertension. A defect in one of the components of this mechanism (e.g., the nitrergic component in the FHR), chronic hypoxia, and/or other pathological triggers may result in deregulation of the suggested homeostatic relaxation of pulmonary arterial smooth muscle.

Although a direct relationship between the nitrergic and vagal sensory CB-IR innervation of NEBs is not clear in Wistar rats, nitrergic innervated NEBs that also receive vagal sensory nerve terminals are apparently more common in FHR lungs, as evidenced by a significantly higher percentage of NEBs that receive both nitrergic and vagal sensory nerve terminals than in Wistar rat lungs. So far, nothing is known about the mechanisms involved and possible functional implications.

TABLE 9
Proportional distribution of nitrergic (nNOS-IR) innervated NEBs along the airways

	n	Mean Percentage of Nitrergic Innervated NEBs in Bronchi	Mean Percentage of Nitrergic Innervated NEBs in Bronchioles	Mean Percentage of Nitrergic Innervated NEBs in Terminal Bronchioles and Respiratory Areas
Wistar rat	7	2.1 ± 0.5%	38.6 ± 4.6%	59.3 ± 4.9%
FHR	7	2.6 ± 2.9%	47.6 ± 5.7%	49.8 ± 5.2%

Data are expressed as mean ± SEM; *n*, number of animals.

TABLE 10
Mean percentage of nitrergic innervated NEBs that additionally receive vagal and/or spinal sensory nerve terminals

	Percentage of Nitrergic Innervated NEBs that Additionally Receive CB-IR Nerve Terminals	Percentage of Nitrergic Innervated NEBs that Additionally Receive CGRP-IR Nerve Terminals
Wistar rat	56.93 ± 2.10% (383/3)	100.0 ± 0.0% (195/2)
FHR	84.68 ± 2.97%* (92/3)	100.0 ± 0.0% (54/3)

Data are expressed as mean ± SEM; numbers in parentheses refer to number of NEBs counted/number of animals studied.
* $P = 0.002$.

In conclusion, the present study presents extensive evidence that NEBs in rat lungs of different strains may be selectively contacted by at least five distinct nerve fiber populations that are both sensory and motor in nature, and have different origins, indicating that NEBs should be regarded as very complex airway receptors that may be capable of accommodating various chemo- and mechanosensory modalities. A strongly reduced number of intrinsic pulmonary nitrergic neurons and of intraepithelial nitrergic nerve terminals that colocalize with NEBs, and that are morphologically linked to spinal sensory CGRP-IR nerve terminals, was demonstrated in FHRs. None of the other parameters of NEBs and their innervation that were compared between Wistar rats and FHRs revealed significant differences, making it rather unlikely that the gross pathologic changes that appear as a consequence of PPH will be due to differences in NEB biology in the FHR. On the other hand, our data of FHRs and Wistar rats, combined with literature data on lung physiology and pharmacology, allow us to speculate on the functional significance of an association between nitrergic nerve terminals and the complex NEB receptors, as a possible mechanism regulating the sensitivity to airway hypoxia. It may be only one of the many quantified parameters that reveals highly significant differences, but NO has been reported to be a key player in the control of chemoreceptor sensitivity in another oxygen sensing system, the carotid body (25). In this way, the hypersensitivity to airway hypoxia observed in FHRs might be associated with a reduced pulmonary nitrergic innervation, possibly via interaction with pulmonary NEBs. The present study of the FHR model for PPH clearly revealed that the interactions between pulmonary NEBs, intrinsic neuronal NO, endogenous neuronal and neuroendocrine CGRP, and oxygen sensing in normal and pathologic lungs deserve further investigation.

TABLE 11
Quantification of pulmonary NEBs and their nitrergic innervation in young adult rats

	Mean Number of NEBs per Animal Based on the Optical Fractionator Method	Mean Percentage of Nitrergic Innervated NEBs
Wistar rat	4961 ± 647 (/4)	8.74 ± 1.05% (3,499/2)
FHR	3960 ± 43 (/2)	1.35 ± 0.62%* (2,630/2)

Data are expressed as mean ± SEM; numbers in parentheses refer to number of NEBs counted/number of animals studied.
* $P = 0.026$.

Acknowledgments: This study was supported by a NOI-BOF grant from the University of Antwerp, and by an IWT grant (SB981363 to I.B.) and an FWO grant (G.0155.01) from the Flemish Government. The authors thank H. De Pauw, D. De Rijck, R. Spillemaeckers, G. Svensson, F. Terloo, J. Van Daele, G. Vermeiren, and D. Vindevogel for their excellent assistance.

References

1. Tschopp, T. B., and M. B. Zucker. 1972. Hereditary defect in platelet function in rats. *Blood* 40:217–226.
2. Kentera, D., D. Susic, V. Veljkovic, G. Tucakovic, and V. Koko. 1988. Pulmonary artery pressure in rats with hereditary platelet function defect. *Respiration (Herrlisheim)* 54:110–114.
3. Sato, K., S. Webb, A. Tucker, M. Rabinovitch, R. F. O'Brien, I. F. McMurtry, and T. J. Stelzner. 1992. Factors influencing the idiopathic development of pulmonary hypertension in the fawn hooded rat. *Am. Rev. Respir. Dis.* 145:793–797.
4. le Cras, T. D., D. H. Kim, S. Gebb, N. E. Markham, J. M. Shannon, R. M. Tuder, and S. H. Abman. 1999. Abnormal lung growth and the development of pulmonary hypertension in the Fawn-Hooded rat. *Am. J. Physiol.* 277:L709–L718.
5. Strange, J. W., J. Wharton, P. G. Phillips, and M. R. Wilkins. 2002. Recent insights into the pathogenesis and therapeutics of pulmonary hypertension. *Clin. Sci.* 102:253–268.
6. Youngson, C., C. Nurse, H. Yeger, and E. Cutz. 1993. Oxygen sensing in airway chemoreceptors. *Nature* 365:153–155.
7. Fu, X. W., C. A. Nurse, Y. T. Wang, and E. Cutz. 1999. Selective modulation of membrane currents by hypoxia in intact airway chemoreceptors from neonatal rabbit. *J. Physiol. Lond.* 514:139–150.
8. O'Kelly, I., R. H. Stephens, C. Peers, and P. J. Kemp. 1999. Potential identification of the O_2-sensitive K^+ current in a human neuroepithelial body-derived cell line. *Am. J. Physiol.* 276:L96–L104.
9. Kemp, P. J., G. J. Searle, M. E. Hartness, A. Lewis, P. Miller, S. Williams, P. Wootton, D. Adriaensen, and C. Peers. 2003. Acute oxygen sensing in cellular models: relevance to the physiology of pulmonary neuroepithelial and carotid bodies. *Anat. Rec.* 270A:41–50.
10. Cho, T., W. Chan, and E. Cutz. 1989. Distribution and frequency of neuroepithelial bodies in post-natal rabbit lung: quantitative study with monoclonal antibody against serotonin. *Cell Tissue Res.* 255:353–362.
11. Brouns, I., D. Adriaensen, G. Burnstock, and J.-P. Timmermans. 2000. Intraepithelial vagal sensory nerve terminals in rat pulmonary neuroepithelial bodies express $P2X_3$ receptors. *Am. J. Respir. Cell Mol. Biol.* 23:52–61.
12. Hartness, M. E., A. Lewis, G. J. Searle, I. O'Kelly, C. Peers, and P. J. Kemp. 2001. Combined antisense and pharmacological approaches implicate hTASK as an airway O_2 sensing K^+ channel. *J. Biol. Chem.* 276:26499–26508.
13. Fu, X. W., D. Wang, C. A. Nurse, M. C. Dinauer, and E. Cutz. 2000. NADPH oxidase is an O_2 sensor in airway chemoreceptors: evidence from K^+ current modulation in wild-type and oxidase-deficient mice. *Proc. Natl. Acad. Sci. USA* 97:4374–4379.
14. O'Kelly, I., A. Lewis, C. Peers, and P. J. Kemp. 2000. O_2 sensing by airway chemoreceptor-derived cells: protein kinase C activation reveals functional evidence for involvement of NADPH oxidase. *J. Biol. Chem.* 275: 7684–7692.
15. Brouns, I., J. Van Genechten, D. W. Scheuermann, J.-P. Timmermans, and D. Adriaensen. 2002. Neuroepithelial bodies: a morphologic substrate for the link between neuronal nitric oxide and sensitivity to airway hypoxia? *J. Comp. Neurol.* 449:343–354.
16. Brouns, I., J. Van Genechten, H. Hayashi, M. Gajda, T. Gomi, G. Burnstock, J.-P. Timmermans, and D. Adriaensen. 2003. Dual sensory innervation of pulmonary neuroepithelial bodies. *Am. J. Respir. Cell Mol. Biol.* 28: 275–285.
17. Adriaensen, D., I. Brouns, J. Van Genechten, and J.-P. Timmermans. 2003. Functional morphology of pulmonary neuroepithelial bodies: extremely complex airway receptors. *Anat. Rec.* 270A:25–40.
18. Lauweryns, J. M., and A. Van Lommel. 1982. Morphometric analysis of hypoxia-induced synaptic activity in intrapulmonary neuroepithelial bodies. *Cell Tissue Res.* 226:201–214.
19. Lauweryns, J. M., and A. Van Lommel. 1986. Effect of various vagotomy procedures on the reaction to hypoxia of rabbit neuroepithelial bodies: modulation by intrapulmonary axon reflexes? *Exp. Lung Res.* 11:319–339.
20. Adriaensen, D., J.-P. Timmermans, I. Brouns, H. R. Berthoud, W. L. Neuhuber, and D. W. Scheuermann. 1998. Pulmonary intraepithelial vagal nodose afferent nerve terminals are confined to neuroepithelial bodies: an anterograde tracing and confocal microscopy study in adult rats. *Cell Tissue Res.* 293:395–405.
21. Springall, D. R., A. Cadieux, H. Oliveira, H. Su, D. Royston, and J. M. Polak. 1987. Retrograde tracing shows that CGRP-immunoreactive nerves of rat trachea and lung originate from vagal and dorsal root ganglia. *J. Auton. Nerv. Syst.* 20:155–166.
22. Brouns, I., L. van Nassauw, J. Van Genechten, M. Majewski, D. W. Scheuermann, J.-P. Timmermans, and D. Adriaensen. 2002. Triple immunofluorescence staining with antibodies raised in the same species to study the complex innervation pattern of intrapulmonary chemoreceptors. *J. Histochem. Cytochem.* 50:575–582.
23. Van Lommel, A., and J. M. Lauweryns. 1993. Neuroepithelial bodies in the Fawn Hooded rat lung: morphological and neuroanatomical evidence for a sensory innervation. *J. Anat.* 183:553–566.
24. Van Genechten, J., I. Brouns, D. W. Scheuermann, J.-P. Timmermans, and D. Adriaensen. 2003. Reduced number of intrinsic pulmonary nitrergic neurons in Fawn-Hooded rats as compared to control rat strains. *Anat. Rec.* 272A:446–453.
25. Prabhakar, N. R., G. K. Kumar, C. H. Chang, F. H. Agani, and M. A. Haxhiu. 1993. Nitric oxide in the sensory function of the carotid body. *Brain Res.* 625:16–22.
26. Gosney, J., D. Heath, P. Smith, P. Harris, and M. Yacoub. 1989. Pulmonary endocrine cells in pulmonary arterial disease. *Arch. Pathol. Lab. Med.* 113: 337–341.
27. West, M. J., L. Slomianka, and H. J. G. Gundersen. 1991. Unbiased stereological estimation of the total number of neurons in the subdivisions of the rat hippocampus using the optical fractionator. *Anat. Rec.* 231:482–497.
28. Howard, C. V., and M. G. Reed. 1998. Unbiased Stereology: Three-Dimensional Measurement in Microscopy. BIOS Scientific Publishers, Oxford, UK.
29. Arvidsson, U., M. Riedl, R. Elde, and B. Meister. 1997. Vesicular acetylcholine transporter (VAChT) protein: a novel and unique marker for cholinergic neurons in the central and peripheral nervous systems. *J. Comp. Neurol.* 378:454–467.
30. Dey, R. D., J. B. Altemus, A. Rodd, B. Mayer, S. I. Said, and R. F. Coburn. 1996. Neurochemical characterization of intrinsic neurons in ferret tracheal plexus. *Am. J. Respir. Cell Mol. Biol.* 14:207–216.
31. Zhu, W., and R. D. Dey. 2001. Projections and pathways of VIP- and nNOS-containing airway neurons in ferret trachea. *Am. J. Respir. Cell Mol. Biol.* 24:38–43.
32. Mazzone, S. B., and B. J. Canning. 2002. Evidence for differential reflex regulation of cholinergic and noncholinergic parasympathetic nerves innervating the airways. *Am. J. Respir. Crit. Care Med.* 165:1076–1083.
33. Prabhakar, N. R. 1999. NO and CO as second messengers in oxygen sensing in the carotid body. *Respir. Physiol.* 115:161–168.
34. Wang, Z. Z., L. J. Stensaas, D. S. Bredt, B. Dinger, and S. J. Fidone. 1994. Localization and action of nitric oxide in the cat carotid body. *Neuroscience* 60:275–286.
35. Kline, D. D., T. Yang, P. L. Huang, and N. R. Prabhakar. 1998. Altered respiratory responses to hypoxia in mutant mice deficient in neuronal nitric oxide synthase. *J. Physiol.* 511:273–287.
36. Martling, C.-R., A. Saria, J. A. Fischer, T. Hökfelt, and J. M. Lundberg. 1988. Calcitonin gene-related peptide and the lung: neuronal coexistence with substance P, release by capsaicin and vasodilatory effect. *Regul. Pept.* 20:125–139.
37. Tjen-A-Looi, S., R. Ekman, H. Lippton, J. Cary, and I. Keith. 1992. CGRP and somatostatin modulate chronic hypoxic pulmonary hypertension. *Am. J. Physiol.* 263:H681–H690.
38. Tjen-A-Looi, S., H. Kraiczi, R. Ekman, and I. M. Keith. 1998. Sensory CGRP depletion by capsaicin exacerbates hypoxia-induced pulmonary hypertension in rats. *Regul. Pept.* 74:1–10.